



Deep Mixing of ^3He : Reconciling Big Bang and Stellar Nucleosynthesis

Peter P. Eggleton, *et al.*

Science **314**, 1580 (2006);

DOI: 10.1126/science.1133065

The following resources related to this article are available online at www.sciencemag.org (this information is current as of June 21, 2007):

Updated information and services, including high-resolution figures, can be found in the online version of this article at:

<http://www.sciencemag.org/cgi/content/full/314/5805/1580>

Supporting Online Material can be found at:

<http://www.sciencemag.org/cgi/content/full/1133065/DC1>

A list of selected additional articles on the Science Web sites **related to this article** can be found at:

<http://www.sciencemag.org/cgi/content/full/314/5805/1580#related-content>

This article has been **cited by** 2 article(s) on the ISI Web of Science.

Information about obtaining **reprints** of this article or about obtaining **permission to reproduce this article** in whole or in part can be found at:

<http://www.sciencemag.org/about/permissions.dtl>

all of these ideas are sufficient to explain the discrepancy between the observed and predicted mass and radius presented here.

References and Notes

1. A. Duquennoy, M. Mayor, *Astron. Astrophys.* **248**, 485 (1991).
2. S. D. Barthelmy *et al.*, *Nature* **438**, 994 (2005).
3. L. Yungelson, M. Livio, *Astrophys. J.* **497**, 168 (1998).
4. B. Willems, U. Kolb, E. L. Sandquist, R. E. Taam, G. Dubus, *Astrophys. J.* **635**, 1263 (2005).
5. B. Paczynski, R. Sienkiewicz, *Astrophys. J.* **248**, L27 (1981).
6. S. B. Howell, S. Rappaport, M. Politano, *Mon. Not. R. Astron. Soc.* **287**, 929 (1997).
7. U. Kolb, *Astron. Astrophys.* **271**, 149 (1993).
8. S. P. Littlefair, V. S. Dhillon, E. L. Martín, *Mon. Not. R. Astron. Soc.* **340**, 264 (2003).
9. R. E. Mennickent, M. P. Diaz, C. Tappert, *Mon. Not. R. Astron. Soc.* **347**, 1180 (2004).
10. K. Beuermann, P. Wheatley, G. Ramsay, F. Euchner, B. T. Gänsicke, *Astron. Astrophys.* **354**, 49 (2000).
11. V. S. Dhillon *et al.*, *Mon. Not. R. Astron. Soc.* **314**, 826 (2000).
12. S. B. Howell, D. R. Ciardi, *Astrophys. J.* **550**, L57 (2001).
13. S. P. Littlefair, V. S. Dhillon, S. B. Howell, D. R. Ciardi, *Mon. Not. R. Astron. Soc.* **313**, 117 (2000).
14. R. E. Mennickent, M. P. Diaz, *Mon. Not. R. Astron. Soc.* **336**, 767 (2002).
15. S. Araujo-Betancor *et al.*, *Astron. Astrophys.* **430**, 629 (2005).
16. A. R. King, K. Schenker, *Astron. Soc. Pac. Conf. Proc.* **261**, 233 (2002).
17. R. E. Taam, H. C. Spruit, *Astrophys. J.* **561**, 329 (2001).
18. U. Kolb, I. Baraffe, *Mon. Not. R. Astron. Soc.* **309**, 1034 (1999).
19. P. Szkody *et al.*, *Astron. J.* **123**, 430 (2002).
20. P. Szkody *et al.*, *Astron. J.* **126**, 1499 (2003).
21. P. Szkody *et al.*, *Astron. J.* **128**, 1882 (2004).
22. P. Szkody *et al.*, *Astron. J.* **129**, 2386 (2005).
23. P. Szkody *et al.*, *Astron. J.* **131**, 973 (2006).
24. K. Horne, T. R. Marsh, F. H. Cheng, I. Hubeny, T. Lanz, *Astrophys. J.* **426**, 294 (1994).
25. J. Wood *et al.*, *Mon. Not. R. Astron. Soc.* **219**, 629 (1986).
26. J. Southworth *et al.*, *Mon. Not. R. Astron. Soc.*, in press; available at <http://xxx.lanl.gov/abs/astro-ph/0609196>.
27. G. Chabrier, I. Baraffe, *Astron. Astrophys.* **327**, 1039 (1997).
28. I. Bildsten, D. Chakrabarty, *Astrophys. J.* **557**, 292 (2001).
29. P. F. L. Maxted, R. Napiwotzki, P. D. Dobbie, M. R. Burleigh, *Nature* **442**, 543 (2006).
30. M. Politano, *Astrophys. J.* **604**, 817 (2004).
31. D. Grether, C. H. Lineweaver, *Astrophys. J.* **640**, 1051 (2006).
32. D. M. Townsley, L. Bildsten, *Astrophys. J.* **596**, L227 (2003).
33. V. Renvoizé, I. Baraffe, U. Kolb, H. Ritter, *Astron. Astrophys.* **389**, 485 (2002).
34. I. Baraffe, U. Kolb, *Mon. Not. R. Astron. Soc.* **318**, 354 (2000).
35. D. Saumon, G. Chabrier, H. M. van Horn, *Astrophys. J. Suppl. Ser.* **99**, 713 (1995).
36. We thank U. Kolb and I. Baraffe for productive discussions. S.P.L., C.A.W., and J.S. are supported by the Particle Physics and Astronomy Research Council (PPARC). T.R.M. acknowledges the support of a PPARC Senior Research Fellowship. B.T.G. acknowledges the support of a PPARC advanced fellowship. Ultracam is supported by PPARC.

Supporting Online Material

www.sciencemag.org/cgi/content/full/314/5805/1578/DC1

Materials and Methods

SOM Text

References

2 August 2006; accepted 25 September 2006

10.1126/science.1133333

Deep Mixing of ^3He : Reconciling Big Bang and Stellar Nucleosynthesis

Peter P. Eggleton,^{1*} David S. P. Dearborn,² John C. Lattanzio³

Low-mass stars, ~ 1 to 2 solar masses, near the Main Sequence are efficient at producing the helium isotope ^3He , which they mix into the convective envelope on the giant branch and should distribute into the Galaxy by way of envelope loss. This process is so efficient that it is difficult to reconcile the low observed cosmic abundance of ^3He with the predictions of both stellar and Big Bang nucleosynthesis. Here we find, by modeling a red giant with a fully three-dimensional hydrodynamic code and a full nucleosynthetic network, that mixing arises in the supposedly stable and radiative zone between the hydrogen-burning shell and the base of the convective envelope. This mixing is due to Rayleigh-Taylor instability within a zone just above the hydrogen-burning shell, where a nuclear reaction lowers the mean molecular weight slightly. Thus, we are able to remove the threat that ^3He production in low-mass stars poses to the Big Bang nucleosynthesis of ^3He .

The standard evolution of a low-mass star (Fig. 1) takes it from a short-lived pre-Main-Sequence (PMS) state, in which it contracts and heats up but has not yet become hot enough to burn its nuclear fuel, to the long-lived MS state in which slow, steady nuclear reactions keep the star in thermal equilibrium. After several gigayears (but depending strongly on mass), the nuclear fuel is exhausted at and near the center, the star becomes cooler, larger, and more luminous, and it starts to climb the red giant branch (RGB). Its outer layers become turbulent and convective, and this surface con-

vection zone (SCZ) penetrates deeply into the star, but the SCZ is forced to retreat again as the fuel-exhausted core, surrounded by a thin, hot nuclear-

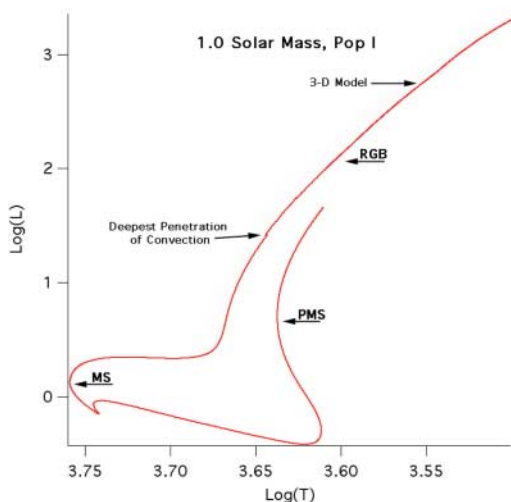


Fig. 1. Evolution of a low-mass Pop I star in a luminosity-temperature diagram. The model was computed in 1D, that is, spherical symmetry was assumed, using the code of (20, 21) with updated equation of state, opacity, and nuclear reaction rates (22). Surface temperature is in kelvins, luminosity in solar units.

¹Institute of Geophysics and Planetary Physics, Lawrence Livermore National Laboratory, 7000 East Avenue, Livermore, CA 94551, USA. ²Physics and Applied Technologies Division, Lawrence Livermore National Laboratory, 7000 East Avenue, Livermore, CA 94551, USA. ³Centre for Stellar and Planetary Astrophysics, Monash University, Australia.

*To whom correspondence should be addressed. E-mail: ppe@igpp.uclnl.org

enough that the ^3He produced is convected into the center of the star and burnt there. In stars of lower mass, however, ^3He accumulates (1) in a broad zone outside the main energy-producing region (Fig. 2A). ^3He is enriched above its assumed initial value [2×10^{-4} by mass (2), the same as its surface value in this plot] in a broad peak extending over nearly half the mass (as well as about half the radius) of the star. The maximum ^3He abundance in this peak is larger than the initial value by a factor of ~ 18 .

On the lower part of the RGB (Fig. 1), a large SCZ develops, which mixes and homogenizes the outer $\sim 0.7 M_\odot$ (Fig. 2B). The surface ^3He abundance is raised from the initial value of 2×10^{-4} to $\sim 1.6 \times 10^{-3}$, that is, by a factor of ~ 8 .

As the star climbs the RGB beyond the point (Fig. 1) where the SCZ penetrates most deeply, the SCZ is diminished by (i) nuclear burning below its base, in a zone that marches outward, and (ii) stellar-wind mass loss from its surface. The evidence for the latter is that the next long-lived stage after the RGB is the horizontal branch (HB), and HB stars appear to have masses that are typically 0.5 to $0.6 M_\odot$, substantially less than the masses of stars capable of evolving to the RGB in less than a Hubble time (3, 4). Process (ii) leads to enrichment of the interstellar medium (ISM) in ^3He (5–7).

Yet the ISM's abundance of ^3He , at $\sim 5 \times 10^{-5}$ by mass, is little different from that predicted by Big Bang nucleosynthesis. This is a major problem (8, 9): Either the Big Bang value is too high, or the evolution of low-mass stars is wrong.

Here, we identify a mechanism by which low-mass stars destroy (on the RGB) the ^3He that they produced during their MS evolution. Although we illustrate this with a star like the Sun, regarding both mass and initial composition, we emphasize that exactly the same applies to low-mass, metal-poor stars [Population II (Pop II)], which may have been more important than metal-rich stars [Population I

(Pop I)] like the Sun throughout the earlier part of Galactic history in determining the ^3He abundance of the interstellar medium. The process is largely independent of mass provided it is fairly low: 1 to $2 M_\odot$ for Pop I and 0.8 to $1.6 M_\odot$ for Pop II.

Once the SCZ has reached its deepest extent, part way up from the base of the RGB, it retreats, and it can be expected to leave behind a region of uniform composition with ^3He enhanced (Fig. 2B). This region is stable to convection according to the usual criterion that the temperature gradient should be subadiabatic and is quite extensive in radius, although small in mass. The H-burning front moves outward into the stable region, but preceding the H-burning region proper is a narrow region, usually thought unimportant, in which the ^3He burns. The reaction that mainly consumes it is $^3\text{He} (^3\text{He}, 2p)^4\text{He}$, which is an unusual reaction in stellar terms because it lowers the mean molecular weight: two nuclei become three nuclei, and the mean mass per nucleus decreases from 3 to 2. Because the molecular weight (μ) is the mean mass per nucleus, but including also the much larger abundances of ^1H and ^4He that are already there and not taking part in this reaction, this leads to a small

inversion in the μ gradient. The inversion is tiny (Fig. 3): It is in about the fourth decimal place. Our three-dimensional (3D) modeling, however, shows the inversion to be hydrodynamically unstable, as we should expect from the classic Rayleigh-Taylor instability.

At a stage (Fig. 3) when the SCZ has just begun to retreat, there is no bump in $1/\mu$, but just a slight distortion at about $0.286 M_\odot$. This is because the ^3He consumption is taking place in a region where there is still a substantial μ gradient left over from earlier history. As the H-burning shell moves out (in mass), though, the ^3He -burning shell preceding it moves into a region of more uniform $^1\text{H}/^4\text{He}$ ratio, so the peak in $1/\mu$ begins to stand out. By the time the leading edge of the shell has moved to $0.29 M_\odot$, there is a clear local maximum in $1/\mu$, which persists indefinitely as the H-burning shell advances and the convective envelope retreats.

At a point somewhat beyond this in the evolution of our 1D star (Fig. 1), we mapped the 1D model onto a 3D model and used the hydrodynamic code “Djehuty” developed at Lawrence Livermore National Laboratory (10–12). [The code is described most fully in (12).] Although Djehuty is designed to deal with an entire star,

Fig. 3. The profile of reciprocal molecular weight ($1/\mu$), as a function of mass in solar units, at three successive times (red, then green 2 million years later, then blue 2 million years later still).

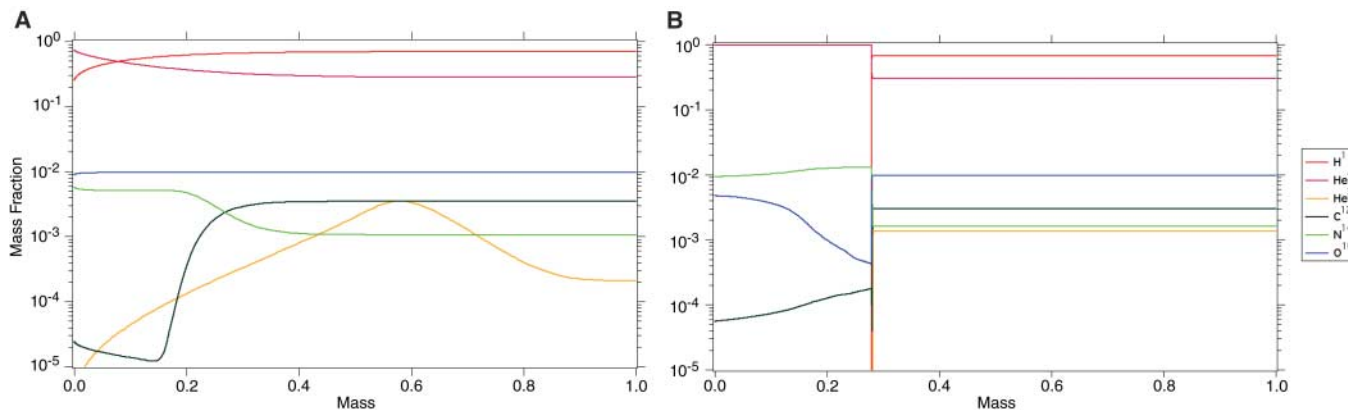
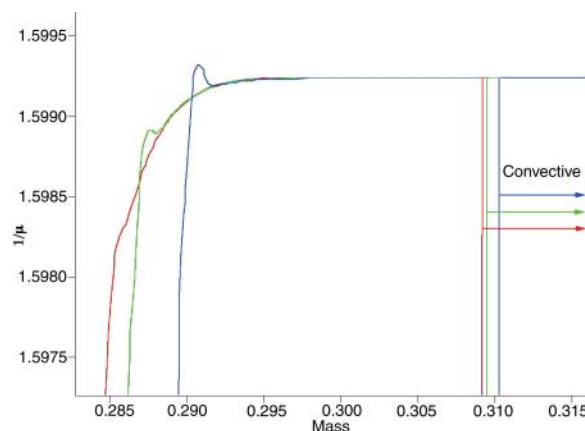
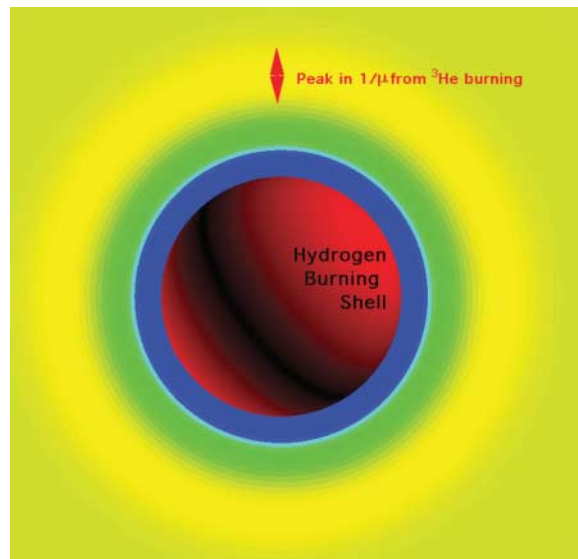


Fig. 2. (A) Profiles of the abundances of certain nuclei in a star that has evolved to roughly the end of the MS (Fig. 1) ($T \sim 5000$ K; $L \sim 2 L_\odot$). ^1H is orange, ^4He is red, ^{16}O is blue, ^{12}C is black, ^{14}N is green, and ^3He is yellow. ^3He shows a major peak where the abundance reaches ~ 18 times the initial

(surface) abundance. **(B)** The same star later, when the SCZ reaches its maximum inward extent (Fig. 1). The ^3He peak has been homogenized to a factor of 8 larger than its initial value. The inert, H-depleted core is about $0.27 M_\odot$.

Fig. 4. A color-coded plot of μ on a cross-section through the initial 3D model. The shell where the μ inversion occurs is the yellow region sandwiched between a yellow-green and a darker green. The inversion is at a radius of $\sim 5 \times 10^7$ m. The base of the SCZ is at $\sim 2 \times 10^9$ m, well outside the frame, and the surface of the star is at $\sim 2 \times 10^{10}$ m.



from center to photosphere, we economized on mesh points by considering only the region below the SCZ. It is important for numerical purposes that the 1D and 3D codes use exactly the same approximations for physical processes, for example, equation of state, nuclear reaction rates, and opacities.

The location of the starting model of the 3D calculation is shown in Fig. 1. If we had been clear before starting the 3D calculation that the $1/\mu$ bump was going to cause mixing, we would have started further down, at the point where the bump first presents itself, which is just above the point labeled “deepest penetration of convection.” It has become clear that our unexpected mixing will begin around here, and in practice we expect that almost all of the ${}^3\text{He}$ in the SCZ will have been consumed by the time the model reaches the point where our 3D calculation started. Because 3D modeling is very expensive of computer time, we have chosen not to redo the calculation for an earlier starting point. Figure 4 is a cross-section of the starting model for the 3D run and shows the μ inversion as a ring well outside the burning shell.

After the early development of the initially spherical shell on which $1/\mu$ has a constant value near its peak (Fig. 5), the surface has begun to dimple after only ~ 800 s, and by 2118 s the dimpling is very marked and the surface has begun to tear. Some points have moved $\sim 2\%$ radially, that is, $\sim 10^6$ m, indicating velocities of ~ 500 m/s. The mean velocity decreases slightly in the passage from the second to the fourth panel. Other spherical shells, well away from the inversion on either side, show no such dimpling, at least until the influence of the inversion has spread to them. A movie of which Fig. 5 is four frames is given as Movie S1 in the Supporting Online Material.

The velocity we see is roughly consistent with the expectation that it should be $v^2 \sim g l \Delta\mu/\mu$, where g is the local gravity and l is the local pressure scale height. The motion appears tur-

bulent and has the effect of diluting the inverse molecular-weight gradient, but it cannot eliminate it. As the turbulent region entrains more of the normally stable region outside it, yet below the normal convective envelope, it brings in fresh ${}^3\text{He}$, which burns at the base of this mixing region, thus sustaining the inverse molecular-weight gradient. Ultimately this turbulent region will extend to unite with the normally convective envelope, so that the considerable reservoir of ${}^3\text{He}$ there will also be depleted. If its speed of ~ 500 m/s is maintained, the time for processed material to reach the classically unstable SCZ is only about 1 month, whereas the time for the H-burning shell to burn through the $\sim 0.02 M_{\odot}$ layer is more than 10^6 years.

The above argument establishes that the mixing in the SCZ is extended below the classical convective limit and that it is very fast compared with the nuclear time scales of either the hydrogen-burning shell or the ${}^3\text{He}$ -burning reaction. We estimate from the nuclear-burning rates that as the hydrogen shell burns outwards the ${}^3\text{He}$ will be destroyed in 16 times as much mass as the hydrogen shell burns through.

We believe that the extra mixing that we have seen gives a satisfactory answer to the problem of matching the ${}^3\text{He}$ abundance of Big Bang nucleosynthesis. Although low-mass stars do indeed produce considerable amounts of ${}^3\text{He}$ on the MS, this will all be destroyed by the substantially deeper mixing that we now expect on the RGB.

Our deeper mixing can also be relevant to further problems. According to the classical models of RGB stars, there is no further modification to the composition in an RGB convective envelope after it has reached its maximum extent early on the RGB. Yet observations persistently suggest that the ratios ${}^{13}\text{C}/{}^{12}\text{C}$ and ${}^{14}\text{N}/{}^{12}\text{C}$ both increase appreciably as one goes up the RGB (13, 14). Both these ratios can be expected to increase only if the material in the envelope is somehow being processed near the H-burning shell. Our

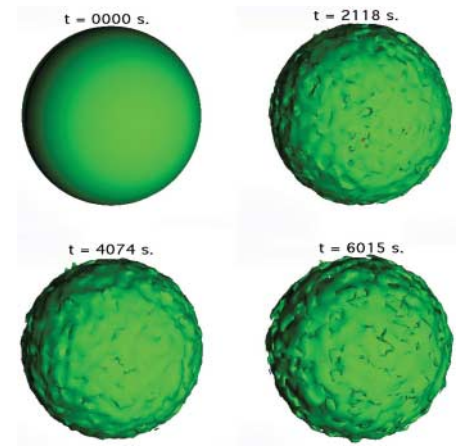


Fig. 5. The development with time of a contour surface of mean molecular weight near the peak in the blue curve of Fig. 3. The contour dimples, and begins to break up, on a time scale of only ~ 2000 s.

model makes this very likely. Although the μ inversion that we find is somewhat above the main part of the H-burning shell, it is not far above, and we can expect some modest processing of ${}^{12}\text{C}$ to ${}^{13}\text{C}$ and ${}^{14}\text{N}$. According to (15), it appears to be necessary for some extra mixing to take place beyond the point on the RGB where the SCZ has penetrated most deeply; that is exactly the point where our mechanism should start to operate. In (15–18) it was suggested that rotation in the region between the SCZ and the hydrogen-burning shell might be responsible for the required mixing. We do not dispute the possible importance of rotation; however, we emphasize that the mechanism we have discovered is not ad hoc but simply arises naturally when the modeling is done in 3D. This mixing occurs regardless of possible variables like rotation and magnetic fields. It seems possible to us that different rates of rotation might vary the efficiency of our process, and we intend to investigate models with rotation in the future.

Correlations between abundance excesses and deficits of various elements and isotopes in the low-mass evolved stars of globular clusters have been reported in (13). Although it is hard to distinguish star-to-star variations that may be due to evolution from those that may be due to primordial variation, we expect our mechanism to lead to substantial evolutionary variations.

Our investigation demonstrates particularly clearly the virtue of attempting to model in 3D, where the motion evolved naturally and to a magnitude that was unexpected.

References and Notes

1. I. Iben Jr., *Astrophys. J.* **147**, 624 (1967).
2. The initial value for ${}^3\text{He}$ that we assumed is somewhat higher than the mass-fraction ($\sim 5 \times 10^{-9}$) implied by (19). This is partly because we assume that primordial deuterium, of comparable abundance, is wholly burnt into ${}^3\text{He}$ before the computation starts. However, the important point is that the great bulk of the ${}^3\text{He}$ in the RG phase is what was synthesized from ordinary hydrogen during the MS phase, not what was there initially. The enrichment factor of 8 that we mention

- above would be a factor of ~ 16 if we started with half as much ^3He , but the abundance level of $\sim 1.6 \times 10^{-3}$ would be very much the same.
- J. Faulkner, *Astrophys. J.* **144**, 978 (1966).
 - J. Faulkner, *Astrophys. J.* **173**, 401 (1972).
 - G. Steigman, D. S. P. Dearborn, D. Schramm, in *Nucleosynthesis and Its Implications on Nuclear and Particle Physics*, J. Audouze, N. Mathieu, Eds. (NATO ASI Series, vol. C163, 1986).
 - D. S. P. Dearborn, D. Schramm, G. Steigman, *Astrophys. J.* **302**, 35 (1986).
 - D. S. P. Dearborn, G. Steigman, M. Tosi, *Astrophys. J.* **465**, 887 (1996).
 - N. Hata *et al.*, *Phys. Rev. Lett.* **75**, 3977 (1995).
 - K. A. Olive, R. T. Rood, D. N. Schramm, J. Truran, E. Vangioni-Flam, *Astrophys. J.* **444**, 680 (1995).
 - G. Bazán *et al.*, in *3-D Stellar Evolution*, S. Turcotte, S. C. Keller, R. M. Cavallo, Eds., ASP conf. 293, p. 1 (2003).

- P. P. Eggleton *et al.*, in *3-D Stellar Evolution*, S. Turcotte, S. C. Keller, R. M. Cavallo, Eds., ASP conf. 293, p. 15 (2003).
- D. S. P. Dearborn, J. C. Lattanzio, P. P. Eggleton, *Astrophys. J.* **639**, 405 (2006).
- N. Suntzeff, in *The Globular Clusters-Galaxy Connection*, G. H. Smith, J. P. Brodie, Eds., ASPC 48, 167 (1993).
- R. P. Kraft, *PASP* **106**, 553 (1994).
- A. Weiss, C. Charbonnel, *Mem. Soc. Astron. Ital.* **75**, 347 (2004).
- A. V. Sweigart, K. G. Mengel, *Astrophys. J.* **229**, 624 (1979).
- C. Charbonnel, *Astrophys. J.* **453**, L41 (1995).
- P. A. Denissenkov, C. A. Tout, *Mon. Not. R. Astron. Soc.* **316**, 395 (2000).
- D. S. Balsear, T. M. Bania, R. T. Rood, T. L. Wilson, *Astrophys. J.* **510**, 759 (1999).
- D. S. P. Dearborn, in *The Sun in Time*, C. Sonett, M. Giampapa, M. Mathews, Eds., ISBN 0-8165-12987-3 (University of Arizona Press, Tucson, AZ, USA, 1991).

- P. P. Eggleton, *Mon. Not. R. Astron. Soc.* **156**, 361 (1972).
- O. R. Pols, C. A. Tout, Zh. Han, P. P. Eggleton, *Mon. Not. R. Astron. Soc.* **274**, 964 (1995).
- We are indebted to R. Palasek for managing the code and for assistance with the graphics. This study has been carried out under the auspices of the U.S. Department of Energy, National Nuclear Security Administration, by the University of California, Lawrence Livermore National Laboratory, under contract W-7405-Eng-48.

Supporting Online Material

www.sciencemag.org/cgi/content/full/1133065/DC1
Movie S1

26 July 2006; accepted 12 October 2006

Published online 26 October 2006;

10.1126/science.1133065

Include this information when citing this paper.

Operation of a DNA Robot Arm Inserted into a 2D DNA Crystalline Substrate

Baoquan Ding and Nadrian C. Seeman*

The success of nanorobotics requires the precise placement and subsequent operation of specific nanomechanical devices at particular locations. The structural programmability of DNA makes it a particularly attractive system for nanorobotics. We have developed a cassette that enables the placement of a robust, sequence-dependent DNA robot arm within a two-dimensional (2D) crystalline DNA array. The cassette contains the device, an attachment site, and a reporter of state. We used atomic force microscopy to demonstrate that the rotary device is fully functional after insertion. Thus, a nanomechanical device can operate within a fixed frame of reference.

Branching DNA has proved to be a very useful and exciting medium for nanotechnology (1). This is a consequence of the programmability of DNA topology and three-dimensional (3D) structure through sequence, combined with the well-defined local structure of intermolecular association that occurs via sticky-

ended cohesion (2). The development of stiff motifs (3) has enabled the self-assembly of DNA components to produce 2D arrays of high quality at atomic force microscopy (AFM) resolutions (4). In a separate but related thread, robust, sequence-dependent DNA nanomechanical devices have also been developed. The insertion of

such nanomechanical devices into 2D arrays results in a nanorobotic system, wherein nanoscale moving parts can be controlled relative to a fixed frame of reference. We report the development of a cassette that contains both a rotary device and the features that enable its insertion into an array at a specific site. A change in the device control sequences or in the insertion sequences would result, respectively, in different controlling elements or in a different site of insertion, all within the context of the same cassette motif.

The PX-JX₂ device is a robust, sequence-dependent DNA machine whose state is controlled by hybridization topology (5). It can assume two structural states [termed PX (paranemic crossover) and JX₂ (paranemic crossover with two juxtaposed sites)] that differ from each other by a half-turn rotation of one end of the molecule relative to the other end. Two different pairs of set strands can bind to the framework

Department of Chemistry, New York University, New York, NY 10003, USA.

*To whom correspondence should be addressed. E-mail: ned.seeman@nyu.edu

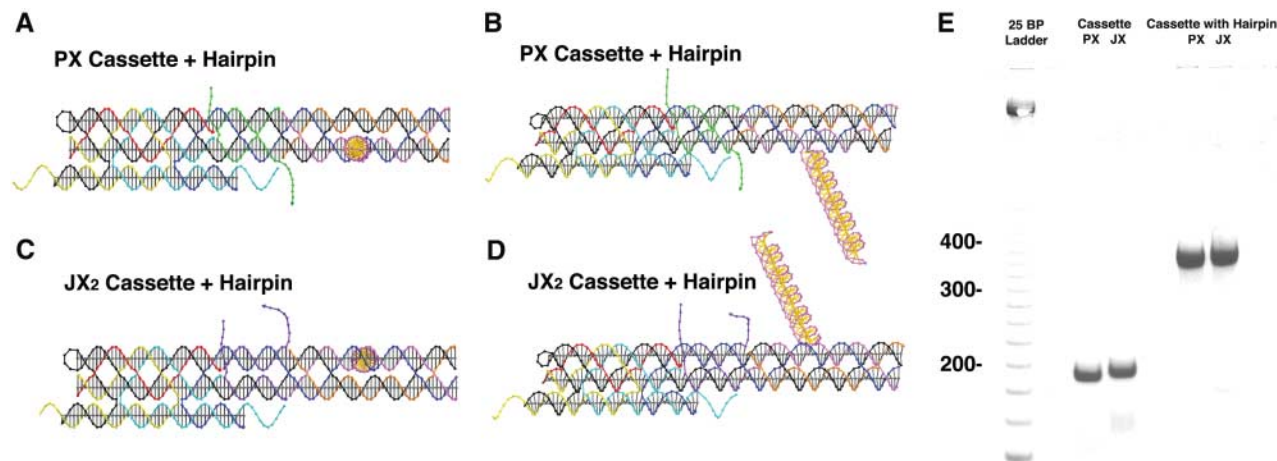


Fig. 1. (A) A view perpendicular to the plane of the cassette in the PX state. The PX state is set by the green strands in the middle of the upper two domains. The reporter hairpin is seen end-on protruding from the plane. The sticky ends on the bottom domain attach the cassette to the 2D array. (B) The same molecule is shown obliquely so the reporter hairpin can be seen. (C) A view similar to (A), except that the cassette is in the JX₂ state, which is set by the purple strands. The

reporter hairpin is now behind the cassette, a point emphasized in (D). All drawings are in a virtual-bond representation produced by the program GIDEON (13). (E) A 5% polyacrylamide gel run in TAEM₉ buffer (3). The two different states are shown both for a cassette without a hairpin and for a cassette including a reporter hairpin. The single bands in each lane indicate that the motifs are stable and monodisperse. BP, base pair.